



Direct measurements of VEGF–VEGFR2 binding affinities reveal the coupling between ligand binding and receptor dimerization

Received for publication, January 25, 2019, and in revised form, April 5, 2019. Published, Papers in Press, April 25, 2019, DOI 10.1074/jbc.RA119.007737

Christopher King and Kalina Hristova¹

From the Department of Materials Science and Engineering, Institute for NanoBioTechnology, and Program in Molecular Biophysics, The Johns Hopkins University, Baltimore, Maryland 21218

Edited by Norma M. Allewell

Vascular endothelial growth factor receptor 2 (VEGFR2) controls angiogenesis and is critically important for normal human development and cancer progression. A recent finding that VEGFR2 can dimerize in the absence of ligand raises the question whether VEGF binds to either VEGFR2 monomers or dimers or to both. Although VEGF–VEGFR2 effective binding constants have been measured, these prior measurements have not discriminated between the association state of the receptor. Because ligand binding is coupled to receptor dimerization, this coupling lends complexity to a seemingly straightforward problem. Here, we unravel this complexity by applying a rigorous thermodynamics approach and performing binding measurements over a broad range of receptor and ligand concentrations. By applying a global fitting procedure to a large data set, we reveal a 45-fold difference between VEGF binding affinities for monomeric and dimeric forms of VEGFR2.

Vascular endothelial growth factor receptor 2 (VEGFR2)² is a 151-kDa member of the receptor tyrosine kinase (RTK) family (1–3). This receptor is expressed on the surface of endothelial cells and controls angiogenesis, the formation of new blood vessels from existing vasculature, as well as vasculogenesis, the *de novo* formation of new blood vessels in tissues (4–6). Thus, VEGFR2 plays a critical role in human development and in cancer progression and is a valuable drug target. Indeed, therapies that inhibit VEGFR2 and angiogenesis would be applicable to many solid tumors, which need oxygen to grow, whereas proangiogenic therapies would be beneficial in the treatment of ischemia, such as in coronary artery disease, stroke, and chronic wounds (7–9).

This work was supported by National Institutes of Health Grant GM068619, National Science Foundation Grant MCB 1712740, and National Science Foundation Graduate Research Fellowship DGE-1232825. The authors declare that they have no conflicts of interest with the contents of this article. The content is solely the responsibility of the authors and does not necessarily represent the official views of the National Institutes of Health.

This article was selected as one of our Editors' Picks.

¹ To whom correspondence should be addressed. Tel.: 410-516-8939; E-mail: kh@jhu.edu.

² The abbreviations used are: VEGFR2, vascular endothelial growth factor receptor 2; VEGF, vascular endothelial growth factor; RTK, receptor tyrosine kinase; EC, extracellular; TM, transmembrane; FSI, fully quantified spectral imaging; scVEGF, single-chain derivative of vascular endothelial growth factor; M, monomers; D, dimers; LM, ligand-bound monomers; LD, ligand-bound dimers; rec, receptors; AF594, Alexa Fluor 594; YFP, yellow fluorescent protein; HEK, human embryonic kidney.

VEGFR2, like most RTKs, consists of an extracellular (EC) domain, a single-pass α -helical transmembrane (TM) domain, and an intracellular kinase domain (10). VEGFR2's EC domain is one of the largest of the RTK family and is composed of seven Ig-like domains, known as subunits D1–D7. Subunits D2 and D3 serve as the binding sites for activating ligands. As in the case of most RTKs, VEGFR2 dimerization and ligand binding are required for its activation (11–13). Dimeric, ligand-bound receptors efficiently cross-phosphorylate each other on specific intracellular tyrosines, which serve as docking sites for intracellular adaptor proteins (1, 2, 11, 14). Adaptor protein binding initiates cytoplasmic signaling cascades controlling endothelial cell survival, proliferation, and motility (1).

The ligands that bind VEGFR2 (VEGF-A and processed forms of VEGF-C and VEGF-D) are released by cells under hypoxic conditions and direct angiogenesis (2, 4, 15). Of these ligands, VEGF-A exhibits the highest binding affinity for VEGFR2 and is considered the most potent angiogenic agent. VEGF-A is a disulfide-linked, antiparallel homodimer (16) that exists as four different isoforms (121, 165, 189, and 206 amino acids long). Although the binding strengths of all VEGF-A isoforms to VEGFR2 are thought to be the same, these isoforms differ in their interactions with the extracellular matrix and the coreceptors on the surface of cells (14, 17–20). VEGF-A121 is the smallest isoform of VEGF-A; however, it contains the full VEGFR2-binding site but lacks the sites mediating the interaction with the extracellular matrix and other coreceptors.

It has been found that VEGFR2 can exist in either a monomeric or a dimeric form on the plasma membrane of cells, even in the absence of ligand (21–23). The existence of VEGFR2 monomers and dimers on the plasma membrane suggests that the formation of VEGF-bound, active dimers can occur through several different pathways (see Fig. 1). In one pathway, the monomeric receptors dimerize on the plasma membrane, upon which a ligand may then bind to the preformed dimer and activate it. Alternatively, a ligand may bind to a monomer of VEGFR2. This liganded monomer may then dimerize with an unliganded VEGFR2 monomer to form an active liganded VEGFR2 dimer. At very high VEGF concentrations, a third pathway exists in which two ligand-bound VEGFR2 monomers can dimerize to form an active dimer upon release of one of the bound VEGF ligands. The prevalence of these pathways in an experiment designed to measure VEGF–VEGFR2 binding affinities will depend on the VEGFR2 ligand-free monomer–

dimer association constant and thus on the total concentration of VEGFR2 on the plasma membrane of cells, on the possibly different binding affinities of VEGF for monomeric and dimeric forms of VEGFR2, and on the concentration of free VEGF in the medium around the cells.

There are previous reports of measurements of effective VEGF binding constants, but they do not discriminate between the association state of the receptor on the surface of the cell because they do not account for the surface density dependence of VEGFR2 dimer formation on the plasma membrane (24–27). Thus, most methods used to assess ligand binding to cell surface receptors cannot provide an answer as to which of the pathways is preferentially utilized in the VEGF-VEGFR2 system. Here, we overcome these prior methodological limitations by employing the fully quantified spectral imaging (FSI) methodology (22) to directly measure the surface density of expressed VEGFR2, the surface density of bound VEGF on the same cell, and the free VEGF concentration in the buffer surrounding the cells. Imaging many cells at different free VEGF concentrations enables the use of a rigorous thermodynamics approach and global fitting to simultaneously determine the separate affinities of VEGF for monomeric and dimeric forms of VEGFR2.

To perform these measurements, we use a commercially available Alexa Fluor 594-labeled version of a recombinant single-chain derivative of vascular endothelial growth factor (scVEGF) (28). Although VEGF-A is a disulfide-linked dimer of two separate chains, scVEGF is an engineered fusion protein that combines two fragments, each composed of amino acids 3–112 of VEGF-A121, that are cloned consecutively in a head-to-tail fashion. By creating a single recombinant protein, Backer and Backer (29) were able to introduce an N-terminal 15-amino-acid tag containing a unique cysteine residue that could be used for site-specific attachment of a single fluorophore despite the presence of 16 native cysteines. scVEGF is a fully functional form of VEGF-A121 as it binds and activates VEGFR2 just like endogenous VEGFs. It is widely used in translational research and has already proven its utility as an imaging and a therapeutic agent (28, 30, 31).

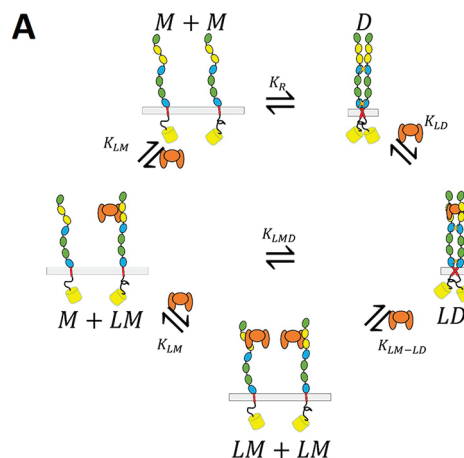
Results

Theory: A thermodynamic cycle for VEGF binding to VEGFR2

We utilize a thermodynamic cycle that accounts for all of the different forms of VEGFR2 that can exist in the absence and presence of VEGF: monomers (M), dimers (D), ligand-bound monomers (LM), and ligand-bound dimers (LD) as shown in Fig. 1A. This model assumes that one molecule of VEGF can bind either a VEGFR2 monomer or a VEGFR2 dimer. This thermodynamic cycle includes all the possible pathways leading from unliganded VEGFR2 monomers to active, VEGF-bound VEGFR2 dimers. Along the *top* of the cycle, VEGFR2 can undergo unliganded dimerization with affinity K_R in units of (receptors/ μm^2)⁻¹.

$$K_R = \frac{[D]}{[M]^2} \quad (\text{Eq. 1})$$

VEGF can then bind to the preformed dimer of VEGFR2 with affinity K_{LD} having inverse molar units (M^{-1}).



$$\begin{aligned} \text{B} \quad K_R &= \frac{[D]}{[M]^2} & K_{LM} &= \frac{[LM]}{[M][L]} \\ K_{LMD} &= \frac{[LD]}{[M][LM]} & K_{LD} &= \frac{[LD]}{[D][L]} \\ K_{LM-LD} &= \frac{[LD][L]}{[LM]^2} \end{aligned} \quad \text{C} \quad \begin{aligned} K_{LMD} &= \frac{K_R K_{LD}}{K_{LM}} \\ K_{LM-LD} &= \frac{K_R K_{LD}}{K_{LM}^2} \end{aligned}$$

Figure 1. A, a thermodynamic cycle describes all of the states of VEGFR2 in the absence and presence of the VEGF ligand. There are three pathways to a ligand-bound VEGFR2 dimer. From *left to right* at the *top* of the cycle, monomeric VEGFR2 undergoes unliganded dimerization with affinity K_R . Free VEGF can then bind to the preformed VEGFR2 dimer. Alternatively, free VEGF can bind to a VEGFR2 monomer. Across the *middle* pathway, this liganded monomer can then bind to an unliganded monomer of VEGFR2, forming a liganded dimer with affinity K_{LMD} . Along the third pathway (*bottom*), two liganded VEGFR2 monomers may dimerize to form a ligand-bound VEGFR2 dimer after release of a bound VEGF molecule into solution. [L] has units of micromolar, and [M] and [D] have units of receptors/ μm^2 . B, mathematical definitions of the association constants shown in A. C, K_{LMD} and K_{LM-LD} can be written in terms of K_R , K_{LM} , and K_{LD} .

$$K_{LD} = \frac{[LD]}{[L]_{\text{free}}[D]} \quad (\text{Eq. 2})$$

Alternatively, a VEGF ligand in solution can bind to a monomer of VEGFR2 with affinity K_{LM} (M^{-1}) (moving from the *top left* position in the thermodynamic cycle down in a *counterclockwise* direction in Fig. 1A).

$$K_{LM} = \frac{[LM]}{[L]_{\text{free}}[M]} \quad (\text{Eq. 3})$$

Moving *right* in the cycle, a VEGF-bound VEGFR2 monomer, LM, can dimerize with an unliganded VEGFR2 monomer, M, again forming the ligand-bound, active dimeric form of VEGFR2 with an affinity of K_{LMD} , having units of (receptors/ μm^2)⁻¹.

$$K_{LMD} = \frac{[LD]}{[LM][M]} \quad (\text{Eq. 4})$$

Traversing further *counterclockwise* around the cycle, under saturating VEGF conditions two liganded VEGFR2 monomers, (LM), can combine to form a liganded dimer of VEGFR2 (LD) only upon release of a VEGF molecule into solution. This process is described by the association constant K_{LM-LD} with units of $\text{M} \cdot (\text{receptors}/\mu\text{m}^2)^{-1}$.

Table 1
Thermodynamic parameters describing VEGF binding to VEGFR2

Association constant	ECTM VEGFR2	Full-length VEGFR2
K_{LM} (M^{-1})	$9.6 \times 10^7 \pm 1.8 \times 10^7$	$9.6 \times 10^7 \pm 1.8 \times 10^7$
K_{LD} (M^{-1})	$4.3 \times 10^9 \pm 0.6 \times 10^9$	$4.3 \times 10^9 \pm 0.6 \times 10^9$
K_R^a ($(\text{rec}/\mu\text{m}^2)^{-1}$)	$3.7 \times 10^{-4} \pm 0.6 \times 10^{-4}$	$3.0 \times 10^{-2} \pm 2.1 \times 10^{-2}$
$K_{LMD} = K_R \cdot K_{LD} / K_{LM}$ ($(\text{rec}/\mu\text{m}^2)^{-1}$)	$1.7 \times 10^{-2} \pm 3.9 \times 10^{-3}$	1.3 ± 0.3
$K_{LM-LD} = K_R \cdot K_{LD} / K_{LM2}$ ($M \cdot (\text{rec}/\mu\text{m}^2)^{-1}$)	$1.7 \times 10^{-10} \pm 1.3 \times 10^{-9}$	$1.4 \times 10^{-8} \pm 1.2 \times 10^{-8}$

^a Measured previously (21, 22).

$$K_{LM-LD} = \frac{[LD][L]_{\text{free}}}{[LM]^2} \quad (\text{Eq. 5})$$

Experimentally, we measure the total surface density of YFP-labeled VEGFR2, [T].

$$[T] = [M] + 2[D] + [LM] + 2[LD] \quad (\text{Eq. 6})$$

We also measure the total bound surface density of scVEGF-AF594 on the same cell.

$$[L]_{\text{bound}} = [LM] + [LD] \quad (\text{Eq. 7})$$

Finally, we measure the free VEGF concentration in the medium surrounding the cells, $[L]_{\text{free}}$.

Using the association constants defined above, we write the total concentration of VEGF2, [T], in terms of the free VEGF concentration and the concentration of monomeric VEGFR2.

$$[T] = 2K_R(1 + [L]_{\text{free}}K_{LD})[M]^2 + (1 + [L]_{\text{free}}K_{LM})[M] \quad (\text{Eq. 8})$$

Next, the bound surface density of VEGF (Equation 7) is written in terms of the monomeric VEGFR2 surface density, the free VEGF concentration, and the association constants.

$$[L]_{\text{bound}} = [L]_{\text{free}}[M](K_{LM} + [M]K_{LD}K_R) \quad (\text{Eq. 9})$$

When [M] is determined from Equation 8 and substituted into Equation 9, Equation 9 provides a link between the measured parameters, K_R , $[L]_{\text{free}}$, and [T], and the unknown binding constants, K_{LM} and K_{LD} . Note that K_R has been measured previously (22), and the measured value is given in Table 1. Thus, there are two unknowns in these experiments, K_{LM} and K_{LD} , and measurements of [T] and $[L]_{\text{bound}}$ for many cells at different $[L]_{\text{free}}$ concentrations yield an overdetermined system of equations that is used to determine the best-fit values of the monomeric and dimeric binding affinities, K_{LM} and K_{LD} .

Experimental measurements of molecular binding affinities

We seek to measure the two-dimensional VEGFR2 surface density in the plasma membranes of HEK293T cells as well as the concentration (surface density) of the bound scVEGF. To achieve this goal, we subject the cells to reversible osmotic swelling as described previously (22, 32, 33). This treatment is required for quantitative determination of the concentration of receptors and bound ligands on the surface of the cells as the complex topology of the resting plasma membrane prevents the conversion of effective 3D concentrations into 2D membrane protein surface densities (22). The osmotic swelling is completely reversible (34–36) and does not change the molecular interactions of VEGFR2 ECTM constructs in the plasma membrane (22). We use a VEGFR2 construct, VEGFR2 ECTM-YFP,

in which the kinase domain is substituted with YFP attached via a $(\text{GGG})_5$ flexible linker to the TM domain (see Discussion below).

Fluorescent AF594-scVEGF is added to the hypotonic swelling medium, and cells expressing VEGFR2 are imaged under two-photon excitation with the OptiMis spectral detection system (37, 38). As shown in Fig. 2A, YFP is intracellularly located, whereas AF594-scVEGF is bound to the extracellular domain of VEGFR2. Fig. 2B shows a schematic of the experimental setup. Measurements of the plasma membrane VEGFR2 surface densities, bound VEGF surface densities, and free VEGF concentrations in the media are performed with the FSI methodology. As described previously (22), FSI enables the measurements of the surface density of fluorophore-labeled membrane proteins in 2–3- μm -size patches by performing two scans, a “donor scan” to excite YFP at 960 nm and an “acceptor scan” to excite AF594 at 800 nm. The fluorescence absorbance and emission spectra of YFP and AF594 are shown in Fig. 2C. FSI also allows for the measurement of the three-dimensional concentration of freely diffusing, fluorescent moieties, in this case free AF594-scVEGF, in the solution surrounding the cells.

Fig. 2, D and E, show three transiently transfected HEK293T cells that have been swollen with hypotonic medium in the presence of AF594-scVEGF. The three cells are each expressing different levels of VEGFR2 ECTM-YFP, as indicated by the differing VEGFR2 ECTM-YFP intensities. Fig. 2D, top, shows the cells under excitation at 960 nm, such that YFP attached to VEGFR2 ECTM is primarily excited. Large stretches of homogeneous membrane fluorescence are visible, with the protein primarily localized in the plasma membrane. Fig. 2D, bottom, shows the same cells under excitation at 800 nm, exciting primarily AF594-scVEGF. AF594-scVEGF is highly concentrated on the surface of the cells, but no Alexa Fluor 594 fluorescence originates from the intracellular space. Thus, the ligand is not endocytosed as expected, primarily because cell swelling inhibits endocytosis (39). Furthermore, the VEGFR2 ECTM construct lacks a kinase domain and does not undergo internalization. On cells with no measurable VEGFR2 ECTM-YFP fluorescence, we see no measurable AF594-scVEGF fluorescence (Fig. 3), indicating that nonspecific binding of VEGF provides a minimal contribution to our measurements.

We measured the surface densities of VEGFR2 ECTM-YFP and bound AF594-scVEGF and the free AF594-scVEGF concentration in 12 independent experiments (at different free ligand concentrations) with a total of 387 cells. The free VEGF concentrations were varied across 3 orders of magnitude, from 0.21 to 42.4 nM, and were measured directly with the FSI method (Fig. 4). These experiments provided a total of 661 data points at the 12 free VEGF concentrations. Fig. 2E shows the

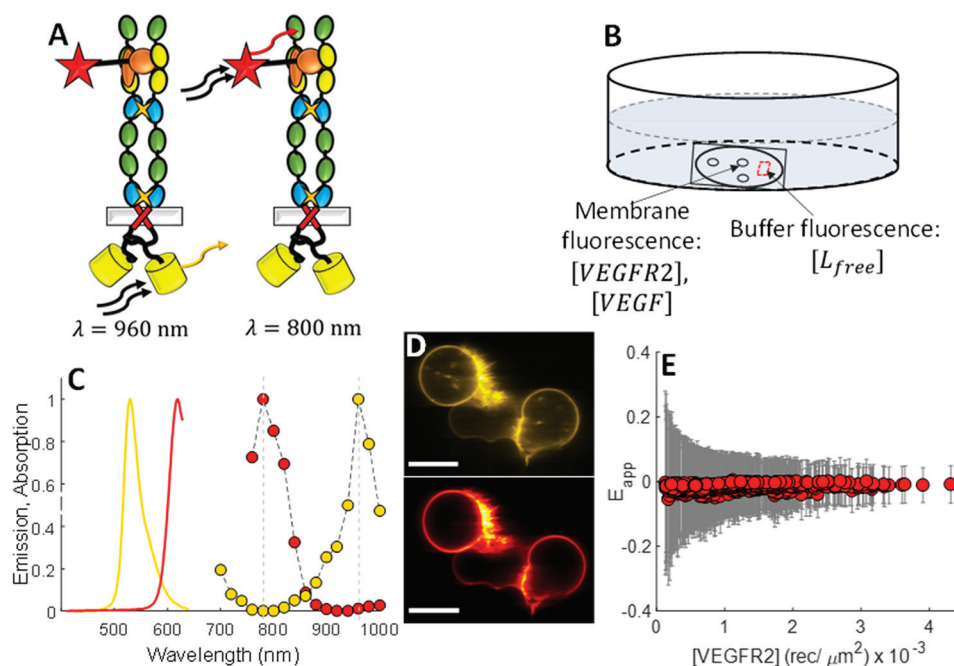


Figure 2. *A*, a cartoon depicting the locations of the fluorophores in a ligand-bound VEGFR2 dimer. YFP is attached to the TM domain of VEGFR2 via a flexible $(\text{GGS})_5$ linker. The labeled ligand, AF594-scVEGF, is commercially available. *B*, the experimental setup for this work. HEK293T cells are seeded in collagen-coated, glass-bottom Petri dishes and are swollen with hypotonic medium containing AF594-scVEGF. Fluorescence from the VEGFR2 ECTM-YFP construct and the bound AF594-scVEGF is then measured on the plasma membrane. The free VEGF concentration in the medium is measured by imaging the free VEGF fluorescence in a region of the dish with no visible cells. *C*, the normalized emission and two-photon absorption of YFP and Alexa Fluor 594 in yellow and red, respectively. The dashed line at 960 nm indicates the typical excitation wavelength for YFP in the FRET scan. The dashed line at 800 nm indicates the excitation utilized in the acceptor scan to excite Alexa Fluor 594. *D*, top, VEGFR2 ECTM- $(\text{GGS})_5$ -YFP fluorescence on the plasma membrane of three HEK293T cells upon excitation at 960 nm. Scale bar, 30 μm . Bottom, bound AF594-scVEGF fluorescence on the plasma membrane upon excitation at 800 nm. Scale bar, 30 μm . *E*, the measured total apparent FRET efficiency and calculated error (E_{app} ; red symbols and gray bars) plotted as a function of the total VEGFR2 surface density. E_{app} is zero for all measured surface densities of VEGFR2, indicating that the intracellular YFP and the extracellularly bound AF594-scVEGF are separated by a distance greater than 10 nm.

measured total apparent FRET efficiency between the intracellular YFP of VEGFR2 ECTM and the extracellularly bound AF594-scVEGF as a function of total VEGFR2 surface density. The FRET efficiency is zero for all concentrations of VEGFR2. This is expected because YFP (the FRET donor) and the AF594 (the FRET acceptor) are further than 10 nm apart when VEGF is bound to the distal region of VEGFR2's EC domain (see Fig. 2A). Indeed, the plasma membrane is ~ 5 nm thick on its own, and the intracellular YFP is a large β -barrel connected to VEGFR2 TM domains via a 15-amino-acid $(\text{GGS})_5$ flexible linker, whereas VEGF is bound to the extracellular D2 and D3 subunits of VEGFR2. Thus, the negligible FRET efficiencies measured for all VEGFR2 surface densities and all free VEGF concentrations serve as an important control for these experiments.

Fig. 5 shows the bound AF594-VEGF surface density plotted as a function of the expressed VEGFR2 ECTM-YFP surface density for each of the 12 different free VEGF concentrations. There is a clear dependence of the binding of VEGF to VEGFR2 on the three-dimensional free scVEGF concentration, where the addition of more free AF594-scVEGF to the media results in more VEGF binding to the VEGFR2 ECTM-YFP construct.

We combined the data from the 12 data sets in Fig. 5 and performed a global fit using Equations 8 and 9 to find the best-fit values of the two adjustable parameters, the binding affinity of AF594-scVEGF for monomeric VEGFR2, K_{LM} , and the bind-

ing affinity of AF594-VEGF for dimeric VEGFR2, K_{LD} (see also Fig. 1). These are the best-fit values of K_{LM} and K_{LD} that globally minimize the error of the model for all 12 data sets, significantly enhancing the accuracy and precision of the fit over that obtained by fitting experiments individually. We find that $K_{\text{LM}} = 9.6e7 \pm 1.8e7 \text{ M}^{-1}$ and that $K_{\text{LD}} = 4.3e9 \pm 0.6e9 \text{ M}^{-1}$ (95% confidence). Thus, there is a 45-fold enhancement of VEGF binding affinity for dimeric VEGFR2 over the affinity of AF594-VEGF for monomeric VEGFR2. The corresponding dissociation constants are 10 nm for VEGF binding to monomeric VEGFR2 and 230 pM for binding of VEGF to dimeric VEGFR2.

The dependence of the bound VEGF as a function of expressed VEGFR2 ECTM surface density for each free VEGF concentration is plotted in the red solid lines of Fig. 5. The dashed red lines indicate the confidence limits on the fit, obtained through propagation of errors on K_{LM} and K_{LD} in Equations 8 and 9, and the 95% confidence limits on K_{LM} and K_{LD} . We see good agreement between the measured data and the best-fit predicted bound VEGF surface densities as a function of VEGFR2 surface densities over 2 orders of magnitude of free VEGF concentrations. Thus, the thermodynamic cycle in Fig. 1 is a model that explains our measured data over a wide range of experimental conditions.

Now that K_{LM} and K_{LD} are determined, we can calculate the dimerization constants K_{LMD} and $K_{\text{LM-LD}}$, provided that the unliganded dimerization constant K_{R} is measured. We have

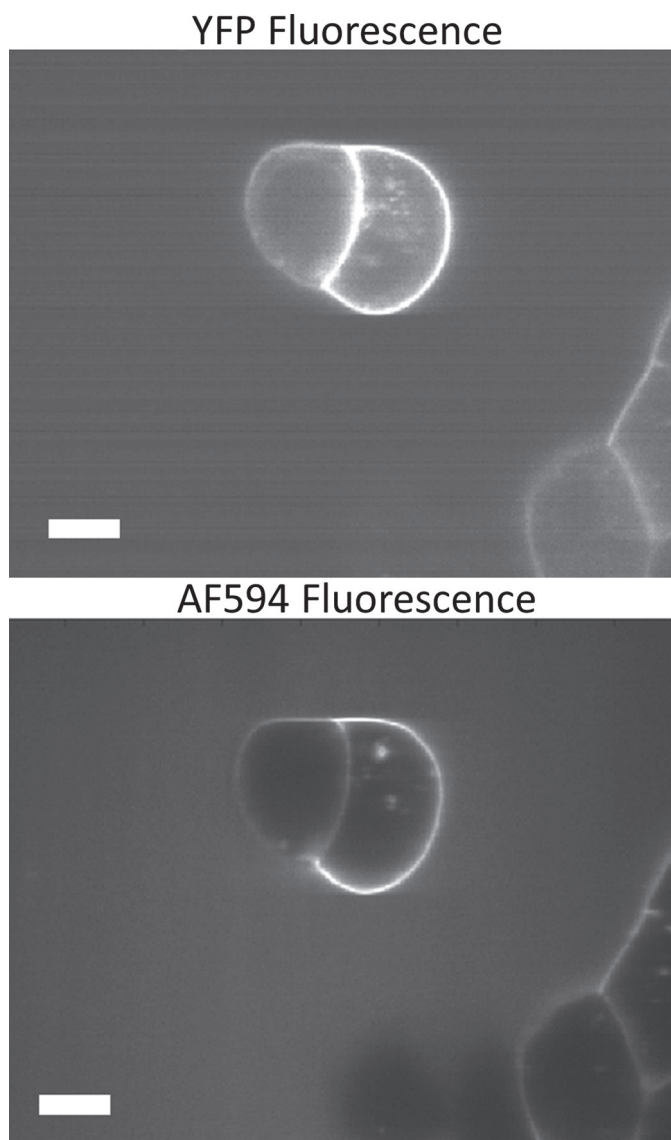


Figure 3. Nonspecific binding of VEGF121 is not detectable on the surface of swollen HEK293T cells. *Top*, VEGFR2 ECTM-YFP is visible at the plasma membrane of five cells upon excitation of YFP at 960 nm. *Bottom*, bound AF594-VEGF121 is visible on all five cells expressing VEGFR2 ECTM-YFP upon excitation at 800 nm. The free VEGF fluorescence in the buffer is also visible. Several “holes” in the buffer VEGF fluorescence indicate the presence of nontransfected HEK cells, but VEGF fluorescence is not detected on these membranes. Scale bar, 10 μm .

previously measured K_R for both the ECTM VEGFR2 and the full-length VEGFR2 in the plasma membrane (21, 22), and we use the measured values for the calculations. The results are shown in Table 1. To calculate K_{LMD} and K_{LM-LD} for the full-length VEGFR2 receptor, we make the assumption that the measured ligand binding constants K_{LM} and K_{LD} are not significantly affected by the presence of the kinase domain positioned on the opposite part of the membrane. Such an assumption is justified as the binding site on the receptor is restricted to subdomains D2 and D3, far from the plasma membrane. Note that although these ligand binding constants are assumed to be independent of the kinase domains, the total bound ligand is enhanced by the presence of the kinase domain as the contacts between the kinase domains in

the VEGFR2 dimer are stabilizing and promote dimerization. Effectively, the presence of the kinase domain enhances VEGF binding because ligand binding and dimerization are coupled.

Because K_R (for unliganded VEGFR2 dimerization) and K_{LMD} (for dimerization of an unliganded monomer with a ligand-bound monomer) have the same units in Table 1, their magnitudes can be directly compared. K_{LMD} is 45 times greater than K_R , indicating that at low VEGF concentrations, dimerization is driven by VEGF binding to VEGFR2 monomers.

Given all the values in Table 1, we can now calculate the probabilities of the full-length VEGFR2 receptor to exist in different dimeric states in the plasma membrane. In particular, Equations 8 and 9 and the previously measured association constant K_R for full-length VEGFR2 dimerization, $3.0 \times 10^{-2} (\text{rec}/\mu\text{m}^2)^{-1}$ (21), can be utilized to predict the abundance of monomers, dimers, VEGF-bound monomers, and VEGF-bound dimers of VEGFR2 for any surface density of the full-length receptor and for any free VEGF concentration.

Fig. 6, A–D, shows the predicted fractions of monomeric VEGFR2, $[M]/[T]$; VEGF-bound monomeric VEGFR2, $[LM]/[T]$; dimeric VEGFR2, $2[D]/[T]$; and VEGF-bound dimeric VEGFR2, $2[LD]/[T]$, as functions of total VEGFR2 surface density and free VEGF concentration. These fractions vary from 0 to 1 and sum up to 1 in all cases. In Fig. 7, we show these distributions at two constant receptor concentrations, 10 and 100 receptors/ μm^2 .

An important prediction of the model is the bell-shaped dependence of the active, ligand-bound, dimeric fraction of VEGFR2 on the free VEGF concentration, shown in Fig. 6D. For fixed VEGFR2 surface densities, the ligand-bound dimeric VEGFR2 fraction increases with increasing VEGF concentration at low VEGF concentrations (up to about 10 nM). At higher concentrations of VEGF, the fraction of ligand bound dimers decreases, whereas the ligand-bound VEGFR2 monomers become dominant. Thus, there exists a ligand concentration for which VEGFR2 activity is the highest. This optimal VEGF concentration is roughly equal to the ligand–monomer dissociation constants, 10 nM, over a broad range of receptor concentrations.

Discussion

The goal of this work was to measure the binding affinity of VEGF for VEGFR2 monomers and VEGFR2 dimers and to characterize the effect of VEGF binding on VEGFR2 dimer stability. We achieve this through direct measurements of the bound VEGF surface density, the VEGFR2 surface density, and the free VEGF concentrations in 12 independent experiments. We then utilized global analysis to fit all the data to the complete thermodynamic cycle in Fig. 1.

The thermodynamic cycle depicted in Fig. 1 describes both receptor–ligand and receptor–receptor interactions, which are coupled, and accounts for all the possible forms of unliganded VEGFR2 and VEGF-bound VEGFR2 that can exist on the plasma membrane of cells. We measured the dissociation constant for VEGF binding to monomeric VEGFR2, K_{LM}^{-1} , as 10 nM and the dissociation constant for

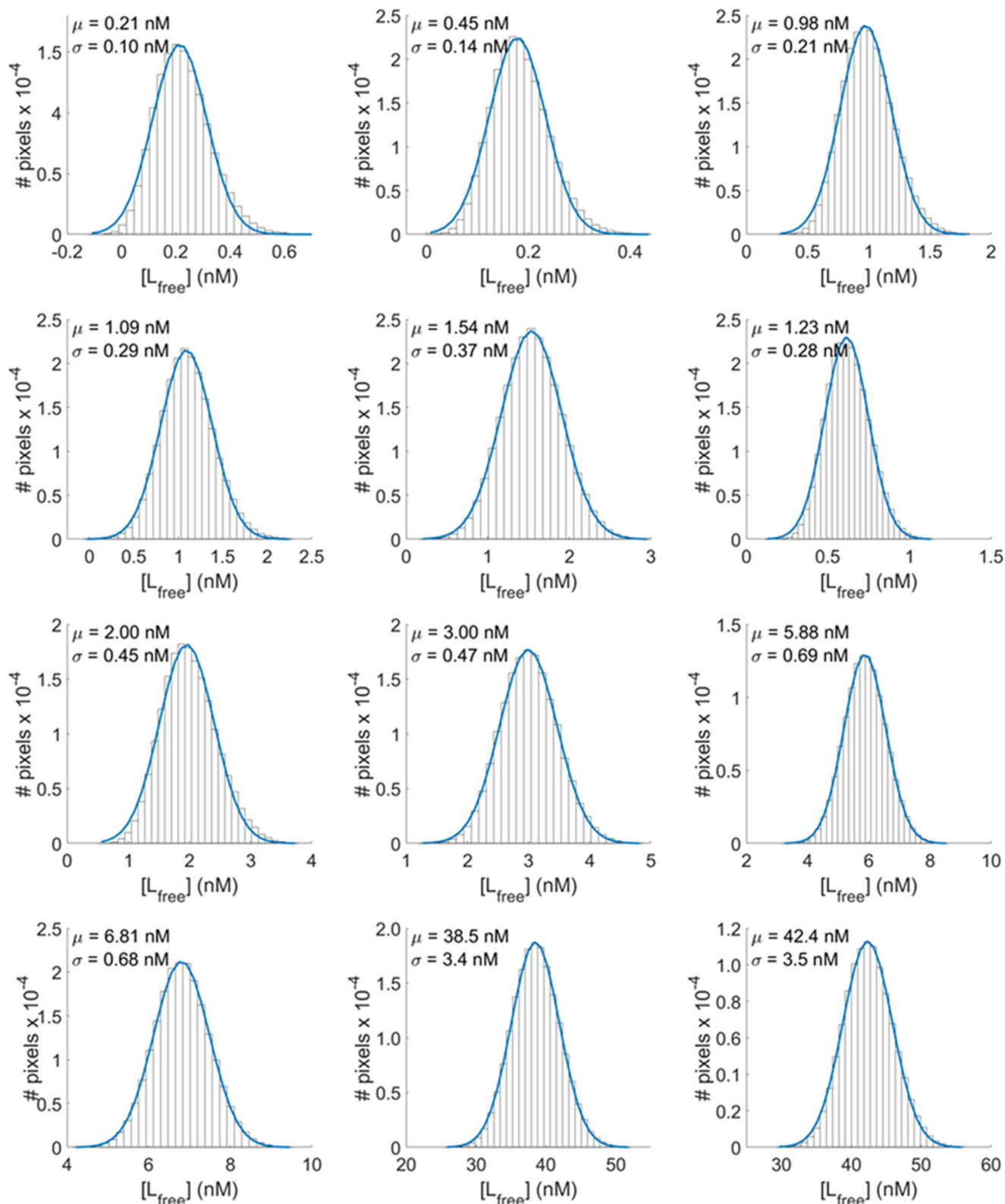


Figure 4. The results of the free VEGF measurements for each of the 12 independent experiments. A Gaussian distribution was fitted to each histogram, yielding the best-fit mean and standard deviations for each measurement.

VEGF binding to dimers of VEGFR2, K_{LD}^{-1} , as 230 pM. Previously, only effective binding constants have been measured, with values ranging from 75 to a few nM (24–27). Here, we find that VEGF binds to both monomers and dimers of

VEGFR2 and that the binding of VEGF to dimeric VEGFR2 is 45 times more favorable than the binding to monomeric VEGFR2, indicating that cooperative interactions stabilize the ligand-bound dimer.

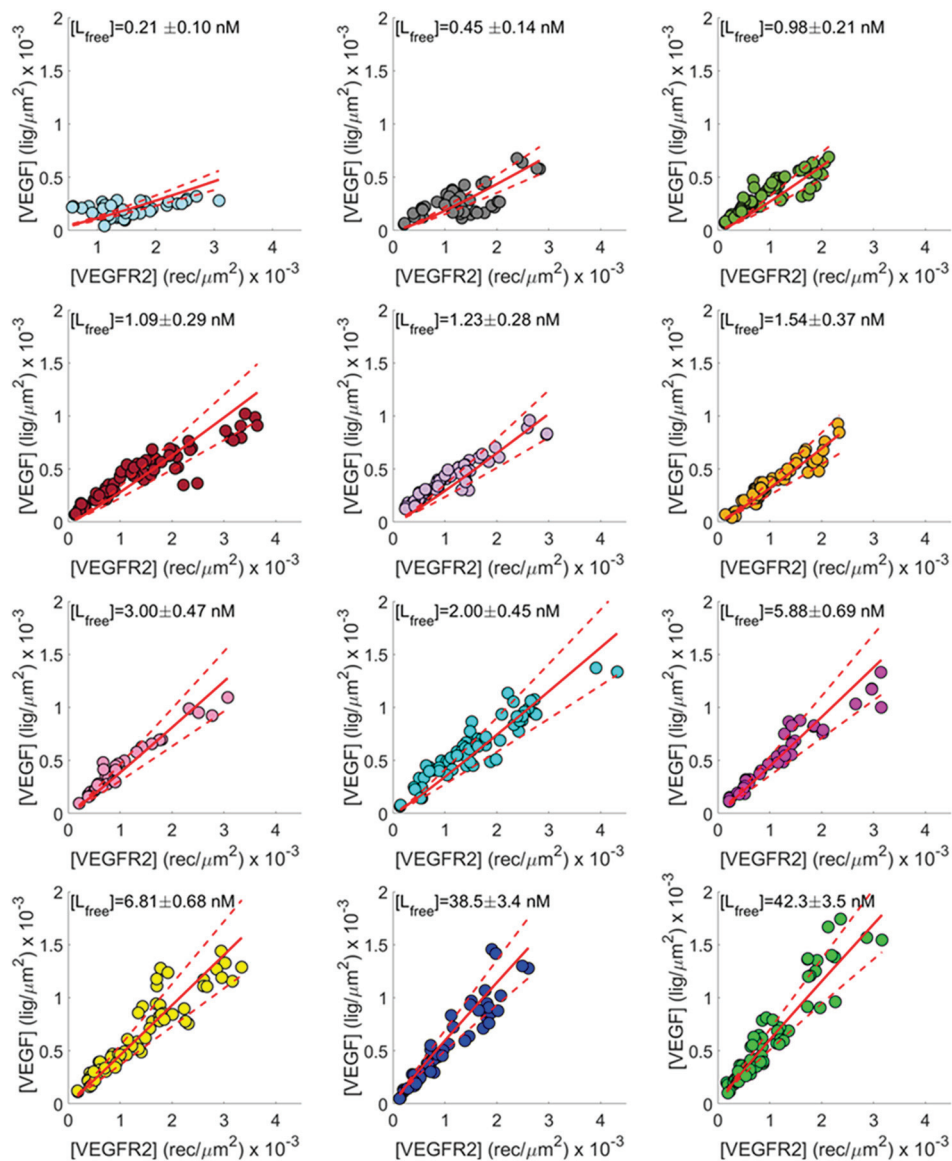


Figure 5. The bound VEGF versus the expressed VEGFR2 surface density and the global best-fit results for 12 independent experiments performed at differing free VEGF concentrations. The best global (simultaneous) fit of the thermodynamic cycle of Fig. 1 to all 12 data sets is plotted with solid lines; the dashed lines indicate the 95% confidence intervals for the fit.

The equilibrium constant describing dimerization in the absence of VEGF, K_R , has been measured previously for full-length VEGFR2 and for truncated VEGFR2 constructs lacking the cytosolic domain (21, 22), and we utilize this knowledge in our experimental design. Full-length VEGFR2 has a very strong propensity for dimerization in the absence of ligand, with a two-dimensional dissociation constant of $33 \pm 23 \text{ rec}/\mu\text{m}^2$. Under the conditions of our experiments (VEGFR2 expression between 100 and 5,000 $\text{rec}/\mu\text{m}^2$), full-length VEGFR2 exists as a nearly constitutive dimeric form, making it difficult for us to measure the affinity of the ligand to the monomeric form of VEGFR2. In contrast, the VEGFR2 ECTM construct, which lacks the intracellular kinase domain, has a much higher dissociation constant and thus lower self-affinity ($2700 \pm 430 \text{ rec}/\mu\text{m}^2$), and the dimeric fraction of VEGFR2 ECTM ranges from 0 to about 80% under the same conditions. The reduced dimer stability of the truncated VEGFR2

ECTM receptor is due to loss of stabilizing contacts that occur between the two intracellular domains in the full-length VEGFR2 dimer (21).

The truncated VEGFR2 ECTM-YFP version offers additional advantages as it does not undergo endocytosis upon ligand binding and is expressed over a broader concentration range than full-length VEGFR2 in transient transfection experiments. Because the contribution of the intracellular domain to unliganded receptor dimerization is known (21), the measurements of K_{LM} and K_{LD} allow us to predict the behavior of the full-length VEGFR2 as a function of VEGFR2 surface density and free VEGF concentrations.

The predictions shown in Fig. 5 document how VEGFR2 surface density and free VEGF concentration control the abundance of the monomers and dimers of VEGFR2 in their VEGF-bound or unbound state. Because VEGFR2 ligand-bound dimers are the signaling-competent dimers, these predictions

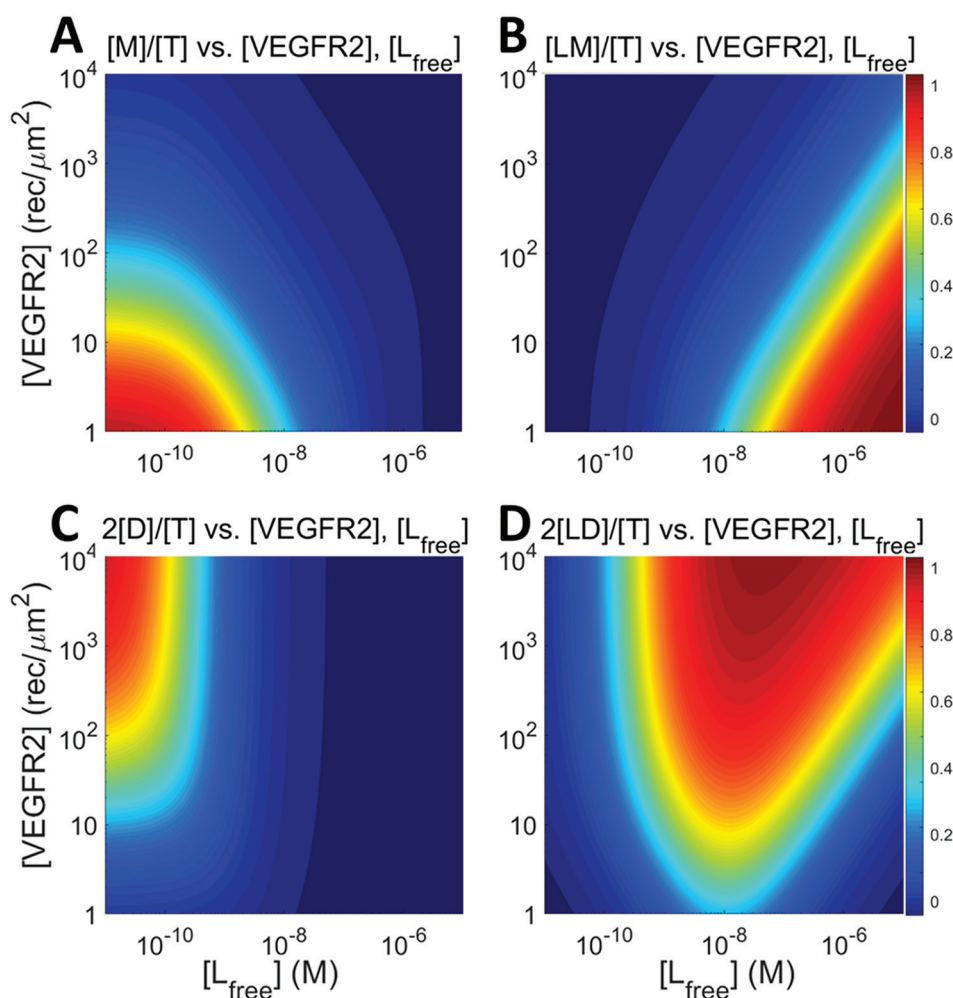


Figure 6. Predicted ligand-free and ligand-bound VEGFR2 fractions for full-length VEGFR2 are plotted as a function of VEGFR2 surface density and free VEGF concentration. A, ligand-free monomeric VEGFR2 fraction. B, ligand-bound monomeric VEGFR2 fraction. C, ligand-free dimeric VEGFR2 fraction. D, ligand-bound dimeric VEGFR2 fraction. At all points, the four fractions sum to 1.

can be used to predict VEGFR2 activity. Indeed, it has been shown that unliganded VEGFR2 dimers are only weakly phosphorylated (21, 40). Ligand binding initiates a conformational switch in the VEGFR2 dimer that is translated through the TM domains to the kinase domains, ultimately ensuring high phosphorylation efficiencies and efficient downstream signaling (21). We see a bell-shaped curve describing the abundance of liganded VEGFR2 dimers as a function of total VEGFR2 surface density. Thus, we predict that high VEGF concentrations suppress VEGFR2 activation. It is noteworthy this behavior is a consequence of the fact that VEGF is a constitutive dimer with symmetric VEGFR2-binding sites unlike other widely studied ligands, such as epidermal growth factor (41). We further predict a threshold of about 10 nM VEGF, equal to the dissociation constant for the monomer, above which an increase in VEGF concentration will decrease the fraction of the liganded VEGFR2 dimer. It is noteworthy that VEGFR2 *in vitro* biochemical studies typically utilize concentrations of about 1 nM VEGF. At 1 nM free VEGF concentration, we predict that about 40% of the receptors exist as liganded dimers, and thus measurements of effective binding constants will be slightly weighted toward the monomeric VEGFR2 binding affinity, K_{LM} .

In the human body, VEGF is believed to act at free VEGF concentrations in the picomolar range (42). At these concentrations, we predict a very low fraction of ligand-bound, active VEGFR2 dimers ($\sim 1\%$) for all surface densities of VEGFR2 (see Fig. 6 or 7). The discrepancy is well-documented in the literature and may be due to the interactions of VEGF with the 3D extracellular matrix as opposed to 2D cell culture or possibly due to the effects of accessory proteins like NRP1 that also bind VEGF on orthogonal binding sites (33, 43, 44). These additional VEGF interactions *in vivo* may prolong signaling, or they may simply serve to enhance the local effective concentration of VEGF or VEGFR2. Fig. 8 shows the x -component of the gradient of the fraction of liganded VEGFR2 dimers (Fig. 6D), a measure of the sensitivity of VEGFR2 activity to changes in free VEGF concentration. We find that the maximum in this gradient occurs at high VEGFR2 surface density where VEGFR2 is primarily dimeric ($>10^3$ receptors/ μm^2) (45, 46) and at very low free VEGF concentrations ($<10^{-11}$ M). It can be expected that this is the “sweet spot” for VEGF to exert its biological action, as small changes in free ligand concentration lead to the largest changes in the population of active, ligand-bound VEGFR2 dimers. Curiously, the free VEGF concentration in this sweet spot is similar to the concentration found *in vivo*.

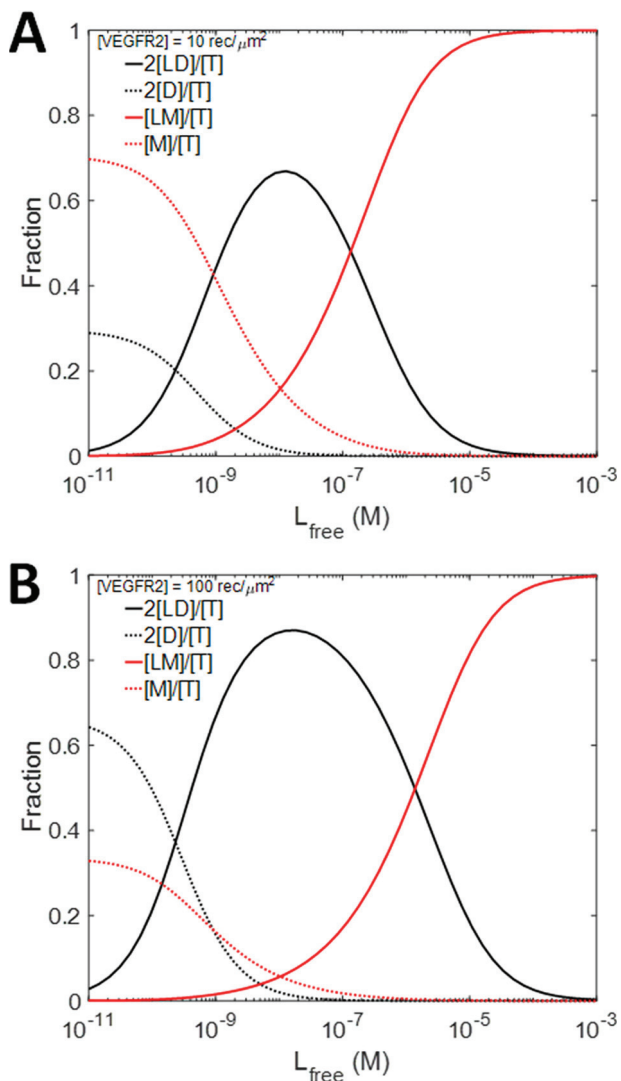


Figure 7. Predicted fractions of ligand-free and ligand-bound monomeric and dimeric full-length VEGFR2 as a function of free VEGF concentration for fixed surface densities of VEGFR2. A, [VEGFR2] = 10 rec/μm². B, [VEGFR2] = 100 rec/μm².

Thus, small changes in the *in vivo* VEGF concentration will lead to the largest possible changes in the fraction of ligand-bound active VEGFR2 dimers. This is a new concept in VEGF research which merits further investigation.

It is noteworthy that the average receptor concentration in endothelial cells is known to be less than 10² receptors/μm² (45, 46), seemingly very different from > 10³ receptors/μm² predicted for this “sweet spot” of VEGF activity. It is possible, however, that VEGFR2 is not distributed homogeneously on the cell surface but instead can reach high local concentrations in membrane domains where VEGFR2 exists as a preformed dimer and is poised to become activated upon ligand binding. Still, the maximum of the gradient occurs where the fraction of ligand-bound VEGFR2 dimers is very low, only about 1%, for *all* VEGFR2 expression levels. This may suggest that the cellular response in the body is exceptionally sensitive to very small numbers of activated VEGFR2 receptors.

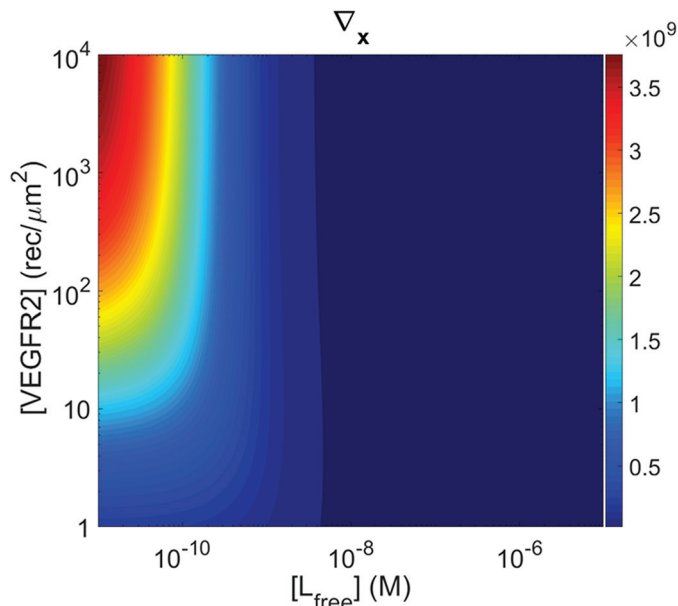


Figure 8. The x-component of the gradient of the fraction of liganded VEGFR2 dimers, a measure of the sensitivity of VEGFR2 activity to changes in free VEGF concentration.

Materials and methods

We utilized scVEGF conjugated to the organic dye Alexa Fluor 594, purchased from SibTech Inc. (catalog number SBT309). The scVEGF conjugate (molecular mass, 28 kDa) consists of two fragments of human VEGF-A121 (amino acids 3–112) cloned head to tail and fused to an N-terminal Cys tag (SibTech Inc., catalog number SBT301). The AF594-scVEGF conjugate is singly labeled in a site-specific manner at the Cys tag and exhibits 95–100% VEGF activity (28). We used a VEGFR2 ECTM construct, labeled with YFP, that has been described previously (22, 23, 33).

Cell culture and transient transfection

The HEK293T cells used in the experiments here were a kind gift from Dr. D. Wirtz, Johns Hopkins University. Transient transfections were performed with a total of 3 μg of plasmid DNA, using Lipofectamine 3000 (Invitrogen) transfection reagent, according to the manufacturer’s protocol.

The cells were serum-starved for at least 12 h prior to the application of reversible osmotic stress and imaging as described (22). At the time of serum starvation, the dishes were blocked with 0.1% BSA to prevent nonspecific binding of VEGF. A 0.1% BSA concentration was maintained throughout the rest of the experiment.

Reversible osmotic swelling, addition of VEGF to cells, and imaging

The hypotonic swelling medium was composed of serum-free medium diluted 1:9 with deionized H₂O, buffered with 25 mM HEPES, supplemented with 0.1% BSA, and 0.2-μm sterile-filtered. Purchased AF594-scVEGF was resuspended in PBS buffer at a concentration of 1 mg/ml and stored in aliquots of ~2.5 μg/aliquot at –20 °C. These aliquots were then used at 1:1, 1:5, 1:10, 1:15, 1:20, 1:25, and 1:50 dilutions and mixed with swelling medium. Just prior to imaging, the starvation medium

was aspirated from the Petri dishes and gently replaced with 1 ml of 37 °C hypotonic swelling medium containing AF594-scVEGF. The cells in each dish were allowed to stabilize for at least 15 min before imaging, and images were acquired at room temperature for up to 2.5 h per dish postswelling.

Image acquisition

The FSI method is utilized in this work to measure the bound AF594-scVEGF surface densities, the VEGFR2 ECTM-(GGG)₅-YFP surface density, and the three-dimensional concentration of free AF594-scVEGF in the buffer surrounding the cells in the dish. The FSI methodology has been described previously in detail (22).

Spectral images were acquired with a two-photon microscope comprising a Mai Tai laser (Spectra Physics), an OptiMis True Line Spectral Imaging system (Aurora Spectral Technologies), and a Zeiss Observer wide-field microscope with a 63× numerical aperture 1.2 water immersion objective as described previously (22). In this work, two different FSI experiments were performed per dish. In the first experiment, two images of each cell were acquired, a donor scan to excite YFP at 960 nm and an acceptor scan to excite AF594-scVEGF at 800 nm. In the second experiment, images of buffer fluorescence, in a region of the dish where no cells were located, were acquired for determination of the free VEGF concentrations.

Fully quantified spectral imaging

Below, we show the equations that are the foundation of the FSI methodology.

$$E_{\text{app}} = F_{\text{RET},\lambda_1}^{\text{D}} / F_{\lambda_1}^{\text{D}} = 1 - F_{\lambda_1}^{\text{DA}} / F_{\lambda_1}^{\text{D}} \quad (\text{Eq. 10})$$

$$[\text{D}] = \frac{F_{\lambda_1}^{\text{D}}}{i_{\text{D},\lambda_1}} = \frac{1}{i_{\text{D},\lambda_1}} \left(F_{\lambda_1}^{\text{DA}} + \frac{Q_{\text{D}}}{Q_{\text{A}}} \left(F_{\lambda_1}^{\text{AD}} - \frac{i_{\text{A},\lambda_1}}{i_{\text{A},\lambda_2}} F_{\lambda_2}^{\text{A}} \right) \right) \quad (\text{Eq. 11})$$

$$[\text{A}] = \frac{F_{\lambda_2}^{\text{A}}}{i_{\text{A},\lambda_2}} = \frac{1}{i_{\text{A},\lambda_2}} \left(F_{\lambda_2}^{\text{AD}} - \frac{i_{\text{D},\lambda_2}}{i_{\text{D},\lambda_1}} F_{\lambda_1}^{\text{AD}} \right) \cdot \left(1 - \frac{i_{\text{A},\lambda_1}}{i_{\text{A},\lambda_2}} \frac{i_{\text{D},\lambda_2}}{i_{\text{D},\lambda_1}} \right)^{-1} \quad (\text{Eq. 12})$$

In these equations, E_{app} is the measured total apparent FRET efficiency, and $F_{\text{RET},\lambda_1}^{\text{D}}$ is the donor fluorescence that is transferred to an acceptor upon excitation in the donor/FRET scan at λ_1 . $F_{\lambda_1,2}^{\text{D,A}}$ is the total fluorescence of the donor or acceptor in the absence of FRET upon excitation at λ_1 or λ_2 . $F_{\lambda_1}^{\text{DA}}$ is the measured fluorescence of the donor in the presence of acceptors, and $F_{\lambda_2}^{\text{DA}}$ is the measured fluorescence of the acceptor, enhanced due to FRET. i_{D,λ_1} and i_{A,λ_2} are the slopes of the solution standard intensity *versus* micromolar concentration curves determined by imaging solution standards of known concentration, described below. Q_{D} and Q_{A} are the quantum yields of the donor and the acceptor.

Equation 12 is directly applied to buffer fluorescence images, and the measured pixel-level concentrations are histogrammed. A Gaussian curve is fit to the data to determine the value of the mean, μ , and the standard deviation, σ , yielding the mean value and error estimate of the free ligand measurement.

For the surface density measurements, the apparent pixel-level fluorophore (receptor and bound ligand) concentrations

calculated during the image analysis are integrated across diffraction-limited membrane segments to determine the 2D surface density from the fluorescence and the calibration curves. To do so, F^{D} , F^{A} , and F^{AD} are integrated (summed) over every pixel selected in the region, $F_{\lambda_1, \text{Reg}}^{\text{D,A}} = \int_{\text{region}}^{\text{D or A}} dA = \sum F_{i,j}^{\text{D or A}}$. The apparent FRET efficiency of the region is then calculated as $E_{\text{app}} = 1 - F_{\lambda_1, \text{Reg}}^{\text{DA}} / F_{\lambda_1, \text{Reg}}^{\text{D}}$.

The total integrated fluorescence intensities for the region, $F_{\lambda_1, \text{Reg}}^{\text{D}}$ and $F_{\lambda_2, \text{Reg}}^{\text{A}}$, are divided by the arc length, s , of the selected region to calculate the average integrated fluorescence per unit length of membrane (in units of pixels). By swelling the cells with osmotic stress, we are able to simplify the complex topology of the membrane and ensure a perpendicular orientation of the membrane with respect to the focal plane. We also assume that the fluorescence originates from an infinitely thin sheet within the width of one pixel, or 254 nm. To obtain the fluorescence that is emitted by fluorophores in a voxel, the integrated fluorescence per unit pixel length is multiplied by the pixel width, 254 nm. By dividing the voxel fluorescence by the average slope, $\langle i_{\lambda_i}^{\text{D,A}} \rangle$, and performing the appropriate unit conversion from micromolar concentrations to receptors per unit area (in units of rec/nm²), the average receptor surface density for the region is calculated as shown below.

$$[\text{D or A}] \left[\frac{\text{rec}}{\text{nm}^2} \right] = \frac{\sum_{s < \langle i_{\lambda_i}^{\text{D,A}} \rangle} F_{i,j}^{\text{D or A}} \left[\frac{\text{counts} \cdot \text{pixel}^2}{[\text{pixel}]} \right] \left[\frac{\text{counts}}{[\mu\text{M}]} \right]^{-1} \cdot 6.022 \cdot 10^{-7} \left[\frac{\text{rec}}{[\mu\text{M}]} \right] \cdot 254 \left[\frac{\text{nm}}{\text{pixel}} \right]}{\quad} \quad (\text{Eq. 13})$$

YFP and Alexa Fluor 594 solution standards

Soluble monomeric YFP with an N-terminal His₆ tag was expressed and purified to near-millimolar concentrations as described (47). Fluorescent protein stocks were buffer-exchanged into PBS buffer with a 20-kDa-molecular-mass-cutoff concentrator (Pierce, catalog number 87751) and filtered with a 0.2- μm syringe filter. Unconjugated Alexa Fluor 594 (A37572) was purchased in lyophilized form from Thermo Fisher Scientific and suspended in PBS buffer. For each imaging session, the stocks were diluted in buffer to micromolar concentrations to produce 100, 75, and 50% fluorescent protein and AF594 solution standards. The solution standard concentrations were measured in a 1-cm-path-length quartz cuvette using NanoDrop 2000C (Thermo Scientific). Molar absorption coefficients of 83,400 and 73,000 M × cm⁻¹ were used to calculate the concentrations of the solution standards from the YFP and AF594 absorption maxima of 514 and 590 nm, respectively. Images of the 100, 75, and 50% solution standards and a PBS buffer-only control were acquired at both excitation wavelengths (800 nm for AF594 and 960 nm for YFP) and used for the calculation of the pixel-level slope values (22). Fig. 2C shows the normalized YFP and AF594-VEGF fluorescence obtained from the membranes of live cells. We see no apparent change in the fluorescence emission properties in the AF594-VEGF or YFP fluorophores on the surface of the cells when compared with that of the solution standards, and the respective emission maxima of 618 and 527 nm remain unchanged.

Author contributions—C. K. software; C. K. formal analysis; C. K. validation; C. K. investigation; C. K. visualization; C. K. methodology; C. K. writing—original draft; C. K. and K. H. conceptualization; K. H. supervision; K. H. funding acquisition; C. K. and K. H. writing—review and editing.

Acknowledgment—We thank M. Paul for reading the manuscript prior to publication.

References

- Olsson, A. K., Dimberg, A., Kreuger, J., and Claesson-Welsh, L. (2006) VEGF receptor signalling—in control of vascular function. *Nat. Rev. Mol. Cell Biol.* **7**, 359–371 [CrossRef Medline](#)
- Shibuya, M., and Claesson-Welsh, L. (2006) Signal transduction by VEGF receptors in regulation of angiogenesis and lymphangiogenesis. *Exp. Cell Res.* **312**, 549–560 [CrossRef Medline](#)
- Koch, S., Tugues, S., Li, X., Gualandi, L., and Claesson-Welsh, L. (2011) Signal transduction by vascular endothelial growth factor receptors. *Biochem. J.* **437**, 169–183 [CrossRef Medline](#)
- Ferrara, N., Gerber, H. P., and Lecouter, J. (2003) The biology of VEGF and its receptors. *Nat. Med.* **9**, 669–676 [CrossRef Medline](#)
- Jeltsch, M., Leppänen, V. M., Saharinen, P., and Alitalo, K. (2013) Receptor tyrosine kinase-mediated angiogenesis. *Cold Spring Harb. Perspect. Biol.* **5**, a009183 [CrossRef Medline](#)
- Qutub, A. A., Mac Gabhann, F., Karagiannis, E. D., Vempati, P., and Popel, A. S. (2009) Multiscale models of angiogenesis. *IEEE Eng. Med. Biol. Mag.* **28**, 14–31 [CrossRef Medline](#)
- Nessa, A., Latif, S. A., Siddiqui, N. I., Hussain, M. A., Bhuiyan, M. R., Hossain, M. A., Akther, A., and Rahman, M. (2009) Angiogenesis—a novel therapeutic approach for ischemic heart disease. *Mymensingh Med. J.* **18**, 264–272 [Medline](#)
- Mac Gabhann, F., Qutub, A. A., Annex, B. H., and Popel, A. S. (2010) Systems biology of pro-angiogenic therapies targeting the VEGF system. *Wiley Interdiscip. Rev. Syst. Biol. Med.* **2**, 694–707 [CrossRef Medline](#)
- Takahashi, H., and Shibuya, M. (2005) The vascular endothelial growth factor (VEGF)/VEGF receptor system and its role under physiological and pathological conditions. *Clin. Sci.* **109**, 227–241 [CrossRef Medline](#)
- Roskoski, R., Jr. (2008) VEGF receptor protein-tyrosine kinases: structure and regulation. *Biochem. Biophys. Res. Commun.* **375**, 287–291 [CrossRef Medline](#)
- Schlessinger, J. (2000) Cell signaling by receptor tyrosine kinases. *Cell* **103**, 211–225 [CrossRef Medline](#)
- Lemmon, M. A., and Schlessinger, J. (2010) Cell signaling by receptor tyrosine kinases. *Cell* **141**, 1117–1134 [CrossRef Medline](#)
- He, L., and Hristova, K. (2012) Physical-chemical principles underlying RTK activation, and their implications for human disease. *Biochim. Biophys. Acta* **1818**, 995–1005 [CrossRef Medline](#)
- Matsumoto, T., and Claesson-Welsh, L. (2001) VEGF receptor signal transduction. *Sci. STKE* **2001**, re21 [CrossRef Medline](#)
- Gerhardt, H., Golding, M., Fruttiger, M., Ruhrberg, C., Lundkvist, A., Abramsson, A., Jeltsch, M., Mitchell, C., Alitalo, K., Shima, D., and Betsholtz, C. (2003) VEGF guides angiogenic sprouting utilizing endothelial tip cell filopodia. *J. Cell Biol.* **161**, 1163–1177 [CrossRef Medline](#)
- Muller, Y. A., Christinger, H. W., Key, B. A., and de Vos, A. M. (1997) The crystal structure of vascular endothelial growth factor (VEGF) refined to 1.93 Å resolution: multiple copy flexibility and receptor binding. *Structure* **5**, 1325–1338 [CrossRef Medline](#)
- Cross, M. J., and Claesson-Welsh, L. (2001) FGF and VEGF function in angiogenesis: signalling pathways, biological responses and therapeutic inhibition. *Trends Pharmacol. Sci.* **22**, 201–207 [CrossRef Medline](#)
- Vempati, P., Popel, A. S., and Mac Gabhann, F. (2014) Extracellular regulation of VEGF: isoforms, proteolysis, and vascular patterning. *Cytokine Growth Factor Rev.* **25**, 1–19 [CrossRef Medline](#)
- Klagsbrun, M., Takashima, S., and Mamluk, R. (2002) The role of neuropilin in vascular and tumor biology. *Adv. Exp. Med. Biol.* **515**, 33–48 [CrossRef Medline](#)
- Zachary, I. C. (2011) How neuropilin-1 regulates receptor tyrosine kinase signalling: the knowns and known unknowns. *Biochem. Soc. Trans.* **39**, 1583–1591 [CrossRef Medline](#)
- Sarabipour, S., Ballmer-Hofer, K., and Hristova, K. (2016) VEGFR-2 conformational switch in response to ligand binding. *Elife* **5**, e13876 [CrossRef Medline](#)
- King, C., Stoneman, M., Raicu, V., and Hristova, K. (2016) Fully quantified spectral imaging reveals *in vivo* membrane protein interactions. *Integr. Biol.* **8**, 216–229 [CrossRef Medline](#)
- King, C., Wirth, D., Workman, S., and Hristova, K. (2017) Cooperative interactions between VEGFR2 extracellular Ig-like subdomains ensure VEGFR2 dimerization. *Biochim. Biophys. Acta Gen. Subj.* **1861**, 2559–2567 [CrossRef Medline](#)
- Terman, B. I., Dougher-Vermazen, M., Carrion, M. E., Dimitrov, D., Armellino, D. C., Gospodarowicz, D., and Böhlen, P. (1992) Identification of the KDR tyrosine kinase as a receptor for vascular endothelial cell growth factor. *Biochem. Biophys. Res. Commun.* **187**, 1579–1586 [CrossRef Medline](#)
- Waltenberger, J., Claesson-Welsh, L., Siegbahn, A., Shibuya, M., and Heldin, C. H. (1994) Different signal transduction properties of KDR and Flt1, two receptors for vascular endothelial growth factor. *J. Biol. Chem.* **269**, 26988–26995 [Medline](#)
- Kilpatrick, L. E., Friedman-Ohana, R., Alcobia, D. C., Ricking, K., Peach, C. J., Wheal, A. J., Briddon, S. J., Robers, M. B., Zimmerman, K., Machleidt, T., Wood, K. V., Woolard, J., and Hill, S. J. (2017) Real-time analysis of the binding of fluorescent VEGF165a to VEGFR2 in living cells: effect of receptor tyrosine kinase inhibitors and fate of internalized agonist-receptor complexes. *Biochem. Pharmacol.* **136**, 62–75 [CrossRef Medline](#)
- Peach, C. J., Kilpatrick, L. E., Friedman-Ohana, R., Zimmerman, K., Robers, M. B., Wood, K. V., Woolard, J., and Hill, S. J. (2018) Real-time ligand binding of fluorescent VEGF-A isoforms that discriminate between VEGFR2 and NRP1 in living cells. *Cell Chem. Biol.* **25**, 1208–1218.e5 [CrossRef Medline](#)
- Anderson, C. R., Rychak, J. J., Backer, M., Backer, J., Ley, K., and Klivanov, A. L. (2010) scVEGF microbubble ultrasound contrast agents: a novel probe for ultrasound molecular imaging of tumor angiogenesis. *Invest. Radiol.* **45**, 579–585 [CrossRef Medline](#)
- Backer, M. V., and Backer, J. M. (2001) Targeting endothelial cells over-expressing VEGFR-2: selective toxicity of Shiga-like toxin-VEGF fusion proteins. *Bioconjug. Chem.* **12**, 1066–1073 [CrossRef Medline](#)
- Blankenberg, F. G., Levashova, Z., Goris, M. G., Hamby, C. V., Backer, M. V., and Backer, J. M. (2011) Targeted systemic radiotherapy with scVEGF/177Lu leads to sustained disruption of the tumor vasculature and intratumoral apoptosis. *J. Nucl. Med.* **52**, 1630–1637 [CrossRef Medline](#)
- Wang, H., Gao, H., Guo, N., Niu, G., Ma, Y., Kiesewetter, D. O., and Chen, X. (2012) Site-specific labeling of scVEGF with fluorine-18 for positron emission tomography imaging. *Theranostics* **2**, 607–617 [CrossRef Medline](#)
- Singh, D. R., Ahmed, F., Sarabipour, S., and Hristova, K. (2017) Intracellular domain contacts contribute to Ecadherin constitutive dimerization in the plasma membrane. *J. Mol. Biol.* **429**, 2231–2245 [CrossRef Medline](#)
- King, C., Wirth, D., Workman, S., and Hristova, K. (2018) Interactions between NRP1 and VEGFR2 molecules in the plasma membrane. *Biochim. Biophys. Acta Biomembr.* **1860**, 2118–2125 [CrossRef Medline](#)
- Singh, D. R., Cao, Q., King, C., Salotto, M., Ahmed, F., Zhou, X. Y., Pasquale, E. B., and Hristova, K. (2015) Unliganded EphA3 dimerization promoted by the SAM domain. *Biochem. J.* **471**, 101–109 [CrossRef Medline](#)
- Singh, D. R., Ahmed, F., King, C., Gupta, N., Salotto, M., Pasquale, E. B., and Hristova, K. (2015) EphA2 receptor unliganded dimers suppress EphA2 pro-tumorigenic signaling. *J. Biol. Chem.* **290**, 27271–27279 [CrossRef Medline](#)
- Sinha, B., Köster, D., Ruez, R., Gonnord, P., Bastiani, M., Abankwa, D., Stan, R. V., Butler-Browne, G., Védie, B., Johannes, L., Morone, N., Parton, R. G., Raposo, G., Sens, P., Lamaze, C., et al. (2011) Cells respond to mechanical stress by rapid disassembly of caveolae. *Cell* **144**, 402–413 [CrossRef Medline](#)
- Raicu, V., Stoneman, M. R., Fung, R., Melnichuk, M., Jansma, D. B., Pisterzi, L. F., Rath, S., Fox, M., Wells, J. W., and Saldin, D. K. (2009) Deter-

- mination of supramolecular structure and spatial distribution of protein complexes in living cells. *Nat. Photonics* **3**, 107–113 [CrossRef](#)
38. Biener, G., Stoneman, M. R., Acbas, G., Holz, J. D., Orlova, M., Komarova, L., Kuchin, S., and Raicu, V. (2013) Development and experimental testing of an optical micro-spectroscopic technique incorporating true line-scan excitation. *Int. J. Mol. Sci.* **15**, 261–276 [CrossRef Medline](#)
 39. Rauch, C., and Farge, E. (2000) Endocytosis switch controlled by transmembrane osmotic pressure and phospholipid number asymmetry. *Biophys. J.* **78**, 3036–3047 [CrossRef Medline](#)
 40. Lamalice, L., Houle, F., and Huot, J. (2006) Phosphorylation of Tyr¹²¹⁴ within VEGFR-2 triggers the recruitment of Nck and activation of Fyn leading to SAPK2/p38 activation and endothelial cell migration in response to VEGF. *J. Biol. Chem.* **281**, 34009–34020 [CrossRef Medline](#)
 41. Wells, A. (1999) EGF receptor. *Int. J. Biochem. Cell Biol.* **31**, 637–643 [CrossRef Medline](#)
 42. Kut, C., Mac Gabhann, F., and Popel, A. S. (2007) Where is VEGF in the body? A meta-analysis of VEGF distribution in cancer. *Br. J. Cancer* **97**, 978–985 [CrossRef Medline](#)
 43. Gu, C., Limberg, B. J., Whitaker, G. B., Perman, B., Leahy, D. J., Rosenbaum, J. S., Ginty, D. D., and Kolodkin, A. L. (2002) Characterization of neuropilin-1 structural features that confer binding to semaphorin 3A and vascular endothelial growth factor 165. *J. Biol. Chem.* **277**, 18069–18076 [CrossRef Medline](#)
 44. Whitaker, G. B., Limberg, B. J., and Rosenbaum, J. S. (2001) Vascular endothelial growth factor receptor-2 and neuropilin-1 form a receptor complex that is responsible for the differential signaling potency of VEGF₁₆₅ and VEGF₁₂₁. *J. Biol. Chem.* **276**, 25520–25531 [CrossRef Medline](#)
 45. Imoukhuede, P. I., and Popel, A. S. (2011) Quantification and cell-to-cell variation of vascular endothelial growth factor receptors. *Exp. Cell Res.* **317**, 955–965 [CrossRef Medline](#)
 46. Imoukhuede, P. I., and Popel, A. S. (2012) Expression of VEGF receptors on endothelial cells in mouse skeletal muscle. *PLoS One* **7**, e44791 [CrossRef Medline](#)
 47. King, C., Sarabipour, S., Byrne, P., Leahy, D. J., and Hristova, K. (2014) The FRET signatures of non-interacting proteins in membranes: simulations and experiments. *Biophys. J.* **106**, 1309–1317 [CrossRef Medline](#)

Direct measurements of VEGF–VEGFR2 binding affinities reveal the coupling between ligand binding and receptor dimerization

Christopher King and Kalina Hristova

J. Biol. Chem. 2019, 294:9064-9075.

doi: 10.1074/jbc.RA119.007737 originally published online April 25, 2019

Access the most updated version of this article at doi: [10.1074/jbc.RA119.007737](https://doi.org/10.1074/jbc.RA119.007737)

Alerts:

- [When this article is cited](#)
- [When a correction for this article is posted](#)

[Click here](#) to choose from all of JBC's e-mail alerts

This article cites 47 references, 13 of which can be accessed free at <http://www.jbc.org/content/294/23/9064.full.html#ref-list-1>